RSC Advances

PAPER

View Article Online
View Journal | View Issue

Cite this: *RSC Adv.*, 2024, **14**, 7052

Kinetic analysis of the crystallization of Y_2O_3 and La_2O_3 doped Li_2O–Al_2O_3–SiO_2 glass

Tao Zheng, [ab] Minghan Li,[b] Yanping Ma*[ab] and Hong Jiang *[ab]

Li_2O–Al_2O_3–SiO_2 (LAS) glass ceramics have a low coefficient of thermal expansion, high mechanical strength, and excellent chemical stability. With advancements in glass ceramics, researchers have explored using LAS glass ceramics with transition metal doping and rare earth doping. Most previous studies have studied the impact of rare earth element doping on crystallization primarily in the context of conventional nucleating agents present in glass. In this study, we aimed to investigate the impact of Y_2O_3 and La_2O_3 on LAS glasses in the presence of undoped nucleating agents. The crystallization mechanism of La_2O_3 and Y_2O_3 doped LAS glass ceramics was studied using differential scanning calorimetry. The crystallization kinetics of the glasses were analyzed using model-free and modeling methods. Moreover, the activation energy of crystallization and the indices of crystallization and growth of glass ceramics were calculated, and the crystalline phase and microstructure of the samples were characterized. All three fractions of the LAS glass showed consistent crystallization under different calculation methods. The glass doped with La_2O_3 and Y_2O_3 exhibited two- or three-dimensional growth during crystallization, promoting crystallization in the LAS glass. The Y_3La_0 sample demonstrated the most favorable crystallization effect. In the presence of an undoped nucleating agent, rare earth elements can enhance glass crystallization; this new idea can be utilized for the development of new materials.

Received 24th October 2023
Accepted 16th January 2024

DOI: 10.1039/d3ra07239h

rsc.li/rsc-advances

1 Introduction

Owing to their unique and exceptional properties, glass ceramics have found extensive application in various fields, such as consumer products, aerospace,[1] biomedical,[1,2] architectural,[3] and electronic devices.[1] Among the many microcrystalline glass systems, Na_2O–CaO–SiO_2,[4] Li_2O–Al_2O_3–SiO_2 (LAS),[5] BaO–Al_2O_3–SiO_2,[6] and MgO–Al_2O_3–SiO_2,[7] LAS is considered the most successful system. LAS glass ceramics exhibit outstanding properties, including a low coefficient of thermal expansion, high mechanical strength, and excellent chemical stability. These remarkable attributes are due to the crystallization of the primary crystalline phases, namely β-quartz solid solution, β-spodumene, and β-eucryptite.[8] With advancements in glass ceramics, researchers have also explored LAS glass ceramics with transition metal doping and rare earth doping.[9,10]

Rare earth ions play an important role as doping elements (modifiers) in various glass systems,[11–13] and they are typically incorporated into glass in the form of oxides. Rare earth elements possess large ionic radii, high coordination numbers, and high ionic field strengths. As a result, doping with rare earth elements can reduce the melting point of glass and enhance the optical and mechanical properties of the microcrystalline glass.[14] Salman *et al.*[10] found that incorporating rare earth oxides into glass ceramics significantly improves the durability and mechanical properties of glass ceramics. In addition, rare earth doping facilitates the promotion of crystallization in glass to some extent. Generally, rare earth ions can be incorporated into glass ceramics as solid solutions,[15] forming new crystalline phases,[16] or they may also exist within the residual glass phase.[17] Researchers have discovered that doping glass with 0.1 wt% of La_2O_3 can effectively lower the crystallization temperature and crystallization activation energy. This process promotes the crystallization of crystals, and La_2O_3 exists in the glass phase in the form of a LaF_3.[17] Y_2O_3 can serve as a network-forming agent in LAS glass systems, effectively promoting glass crystallization.[18] The inclusion of Y_2O_3 influences the crystallization behavior of LAS glasses, particularly when nucleating agents are present.[19–23] Wei and Jin-Shan discovered that rare earth doping hinders the transformation of β-quartz to β-spodumene.[24] Li *et al.* utilized Y_2O_3/La_2O_3 instead of SiO_2 (ref. 25) to enhance the properties of LAS glass ceramics, successfully developing glass ceramics with a high refractive index and elastic modulus. Additionally, co-doping rare earth elements can induce a shift in the crystallization peak of glass towards higher temperatures. Nevertheless, in most previous studies, the impact of rare earth element doping on crystallization has been investigated primarily in the context of conventional nucleating agents (such as TiO_2, ZrO_2, and

[a]State Key Laboratory of Marine Resources Utilization in South China Sea, Hainan University, Haikou 570228, China. E-mail: myp@hainanu.edu.cn; sumian0313@163.com

[b]Special Glass Key Lab of Hainan Province, Hainan University, Haikou 570228, China

P_2O_5) present in the glass. In the presence of these conventional nucleating agents, Prnová *et al.* observed that glasses doped with La_2O_3 exhibited crystal crystallization with two-dimensional growth and three-dimensional growth nucleation mechanisms.[26] A relatively high proportion of vanadium oxide can be used as a nucleating agent to crystallize sub-stable $CaAl_2Si_2O_8$ in CAS glasses.[27] Although La_2O_3 addition has no effect on the main crystal phase type of the microcrystalline glass, it can effectively promote the nucleation and crystallization of the matrix glass at a lower temperature.[28] The introduction of yttrium oxide reduces the viscosity and melting temperature. Moreover, yttrium oxide plays an important role in regulating the parameters of crystallization kinetics and controlling the crystal size and crystallinity.[29] Shakeri[30] found that an increase in Y_2O_3 content improved the three-dimensional growth of crystals considerably.

Differential thermal analysis is a common tool for studying the kinetic theory of crystallization. During the crystallization process, determining kinetic parameters, such as the activation energy for crystallization (E) and the finger-forward factor (A), and identifying the reaction model is crucial. Researchers can employ both isothermal and non-isothermal methods to determine the crystallization activation energy and the kinetic model of glass. Non-isothermal methods are further categorized into model-fitting methods and iso-conversion methods (model-free methods). A combination of the model-free and model-fitting methods can better describe the crystallization behavior of glass.

Most previous studies focused on the presence of conventional nucleating agents. In this study, we aimed to investigate the impact of Y_2O_3 and La_2O_3 on LAS glasses under the condition of undoped nucleating agents. Additionally, we compared and analyzed the effects of La_2O_3 and Y_2O_3 and the co-doping of La_2O_3 and Y_2O_3 on the crystallization of LAS glass. The addition of traditional nucleating agents is avoided during the preparation of glass ceramics to maintain the unique structural characteristics and properties of microcrystalline glass; this can help achieve the desired microcrystallization effect. The study of the effect of rare earth element doping on the crystallization of LAS glass without the addition of traditional nucleating agents can provide new ideas for future research and development of new materials.

2 Experimental design

2.1 Preparation of glass ceramics

Alumina, silica sand, magnesium carbonate, sodium carbonate, sodium chloride, and lithium carbonate (purity: 99%; obtained from Macklin) were used as raw materials for the glass composition. The required amounts of these ingredients, as indicated in Table 1, were accurately calculated and weighed. They were thoroughly mixed to achieve different ratios of glass ingredients. Subsequently, the mixed ingredients were placed in a muffle furnace and heated to 1550 °C. The high temperature was maintained for 2 h to melt and homogenize the glass. The homogenization of the glass liquid is mainly achieved *via* the molecular diffusion motion due to the uneven composition, convection motion due to temperature differences, and agitation due to rising air bubbles.[31] After the melting process, the molten glass liquid was carefully poured into a pre-prepared graphene mold. This mold containing the glass liquid was then transferred to an annealing furnace, the temperature of which was set to 600 °C and maintained for 2 h continuously. Conventional nucleating agents are most effective in promoting crystallization at concentrations of 0–3 mol, whereas rare earth oxides in this concentration range reduce the viscosity of the glass. Three LAS glass ceramics samples, Y_0La_3, $Y_{1.5}La_{1.5}$, and Y_3La_0, were successfully prepared. These samples were processed under specific nucleation and crystallization temperature conditions.

2.2 Characterization of glass ceramics

Heating experiments were carried out on glass powders using a differential scanning calorimeter (NETZSCH STA 449 F3 STA449F3A-1664-M) from room temperature to 1200 K in nitrogen atmosphere using different heating rates ($\alpha = 5, 10, 15,$ and 20 K min^{-1}). The peak crystallization temperature (T_p) of the glass was determined by analyzing the differential scanning calorimetry (DSC) curves, with an error of measurement of ± 1 K. The crystalline phases of the heat-treated samples were identified, and their crystallinity was estimated using Cu Kα radiation in an X-ray powder diffractometer (SmartLab, RIGAKU). The X-ray diffraction (XRD) patterns were recorded in the 2θ range from 5–70° with a step size of 0.02° per step and 0.2 s per step. The XRD data were analyzed using the Jade software. In addition, the microstructure of the glass-ceramics samples was observed using a field emission scanning electron microscope equipped with an energy dispersive spectrometer (MIRA3, TESCAN), and the measured surfaces of the samples were polished and eroded in 5.0% (mass concentration) HF acid solution for 30 s. The samples were then cleaned with water. The eroded surfaces were cleaned with deionized water; the samples were dried and gold sprayed.

3 Results and discussion

3.1 Differential scanning calorimetry

In the non-isothermal DSC study, the temperature of the samples was increased from 25 °C to 1200 °C at a heating rate of 5, 10, 15, and 20 °C min^{-1}. Fig. 1 illustrates the range of exothermic crystallization peaks (T_p), which ranges from 600–900 °C. The crystallization peaks (T_p) of the glasses shifted towards higher temperatures with increasing heating rates. As shown in the DSC plots for the three glass fractions, as the Y_2O_3 content increased, the crystallization peak temperature

Table 1 Chemical composition of glass

(mol/%)	SiO_2	Al_2O_3	Y_2O_3	La_2O_3	MgO	Na_2O	Li_2O
Y_0La_3	65	10	0	3	7	5	10
$Y_{1.5}La_{1.5}$	65	10	1.5	1.5	7	5	10
Y_3La_0	65	10	1.5	1.5	7	5	10

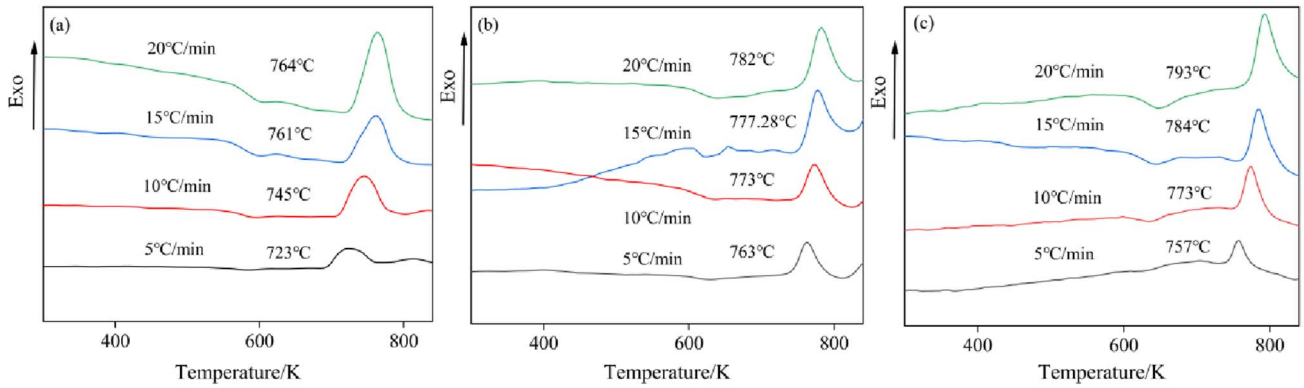

Fig. 1 (a–c) Non-isothermal DSC results of Y_0La_3, $Y_{1.5}La_{1.5}$, and Y_3La_0 samples at 5, 10, 15 and 20 °C min^{-1}.

gradually increased. This phenomenon may be attributed to the fact that the glass samples exhibit more ionic bonding and less covalent bonding in the microstructure of [SiO_4] tetrahedra.[32] Moreover, the incorporation of rare earth elements into the glass network structure as network-forming bodies is challenging, and hence, the rare earth elements can occupy only the network interstices. The obtained DSC crystallization peaks at different heating rates were utilized to calculate the kinetic parameters for the three different glass components, including the activation energy of crystallization and the growth index of crystallization. These calculations were performed to predict the crystal growth mechanism.

3.2 X-Ray diffraction and scanning electron microscopy analysis

Fig. 2 shows the XRD patterns of the LAS glass ceramics obtained using a two-step heat treatment method. The analysis of the XRD plots, conducted using JADE software, revealed that all three component glass samples, which were not doped with nucleating agents, precipitated a β-quartz solid solution ($LiAlSi_3O_8$) during the heat treatment. The addition of rare earth elements induces a separation of the silica-rich $LiAlSi_3O_8$ and a consequent formation of the $LiAlSi_3O_8$ primary crystalline phase in the matrix glass. The viscosity of the glass decreases due to the phase splitting effect of the rare earth ions, and the atoms can easily migrate in the vitreous solution, leading to the growth of the crystalline phase formation. The calculations further demonstrated that the component glass sample doped solely with the Y element exhibited the highest level of crystallinity, whereas the sample doped solely with La had the lowest crystallinity. As shown in Fig. 3, spherical crystals with a grain size of approximately 1 μm were observed. Furthermore, EDS tests were conducted on the spherical crystals present in the three component glass samples, identified as point 1 in Fig. 3a–c. The results—displayed in Fig. 3d–f—show the presence of Al, Si, and O elements within these spherical crystals. These results, combined with the XRD results, indicate that the observed spherical crystals correspond to the $LiAlSi_3O_8$ crystalline phase.

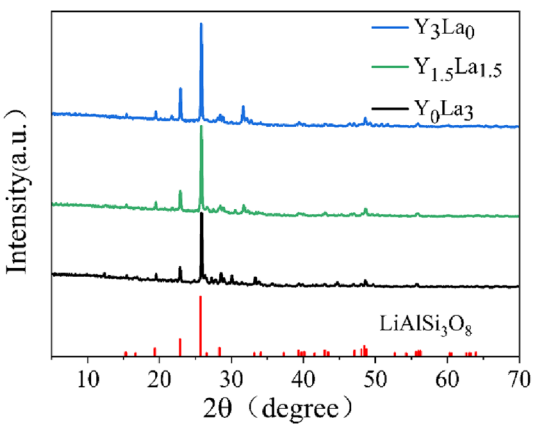

Fig. 2 (a–c) XRD phase identification of glass samples with different components after crystallization.

3.3 Kinetic analysis

3.3.1 Non-isothermal method for kinetic analysis. Crystallization kinetics play a crucial role in understanding the transition of a material from the glassy to the crystalline state. Two essential parameters in crystallization kinetics are the crystallization activation energy (E_c) and the Avrami index (n), which are useful for gaining insight into the crystallization behavior of glassy materials. The crystallization activation energy (E_c) represents the energy barrier that atoms must overcome during the transition from the glassy to the crystalline state. For solid-phase reactions under non-isothermal conditions, the standard nucleation growth model[33–35] known as the Johnson–Mehl–Avrami model, is commonly employed. Model-fitting methods are well known for their simplicity in providing kinetic triplets, although they cannot uniquely model the entire reaction. This model describes the calorimetric data of DSC in terms of the crystallinity fraction (x) as a function of time (t), according to the following expression (1):

$$x = 1 - \exp[-(kT)^n] \quad (1)$$

where n is the Avrami index that reflects the nucleation and crystal growth mechanisms as well as the crystal morphology, and the parameter k is the crystallization kinetic reaction rate,

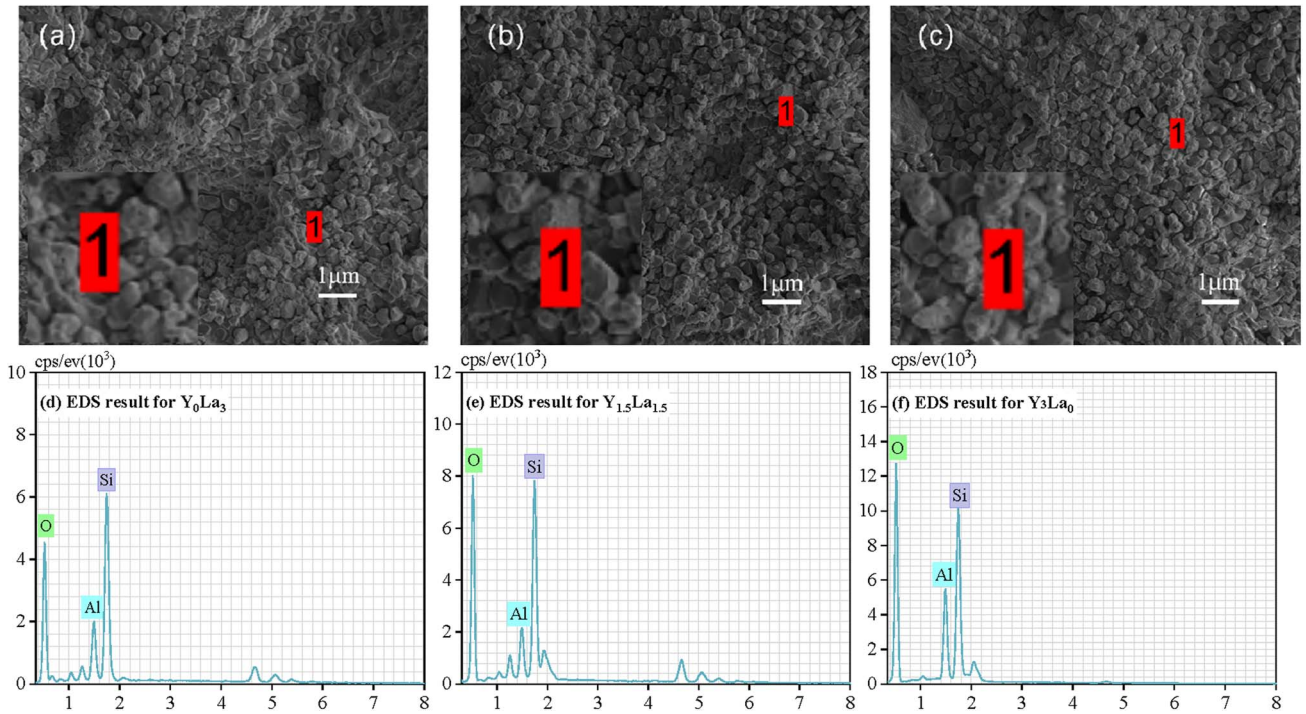

Fig. 3 (a–c) SEM-BSE phase morphology of Y_0La_3, $Y_{1.5}La_{1.5}$, and Y_3La_0 crystalline samples, (d–f) Phase identification results corresponding to 1 point in Y_0La_3, $Y_{1.5}La_{1.5}$ and Y_3La_0 samples.

which describes the growth and nucleation rate of precipitated crystals.

$$k = k_0 \exp\left(-\frac{E}{RT}\right) \quad (2)$$

Here, k_0 is the activation energy (frequency) factor, E is the activation energy of crystallization during glass crystallization, R is the gas constant, and T is the absolute temperature. On the basis of the Johnson–Mehl–Avrami–Kolmogorov theoretical model, several equations (*e.g.*, Matusita–Sakka method,[36] Ozawa method,[37] Kissinger method[38]) can be derived to evaluate the crystallization kinetic parameters. We chose the classical Kissinger method to analyze the crystallization kinetics of glass.

3.3.2 Kissinger model. In classical nucleation, the nucleation and growth phases occur around the glass transition temperature. Therefore, the Kissinger model represents a scenario in which the reaction rate dx/dt reaches its maximum at T_p, while the conversion x maintains a constant value, x_p, for different heating rates α. Based on the above definitions, E_c is calculated in the Kissinger model using the following equation:

$$\ln\left(\frac{Tp^2}{\alpha}\right) = \frac{E_c}{RT_p} + C_1 \quad (3)$$

where C_1 is a constant, E_c is calculated from the slope of the straight line of $\ln(T_p^2/\alpha) - 1000/T_p$ as shown in Fig. 4; the value of R^2 obtained from the fit was 0.99. The activation energies of the three-component glass samples (Y_0La_3, $Y_{1.5}La_{1.5}$, and Y_3La_0), obtained from Fig. 4, were 133.24, 354.81, and 180.23 kJ mol^{-1}, respectively.

The Avrami index (crystallization growth index) can be calculated using the following equation:[39]

$$n = \frac{2.5}{\Delta T} \times \frac{RT_p^2}{E_c} \quad (4)$$

where ΔT corresponds to the half-height width of the exothermic crystallization peak in the DSC curve, as shown in Fig. 2. The values of the growth indices n for Y_0La_3 and $Y_{1.5}La_{1.5}$ are less than 2, indicating that these two samples undergo one-dimensional crystallization from the beginning to the end. The values of n for Y_3La_0 are greater than 3, which indicates that the

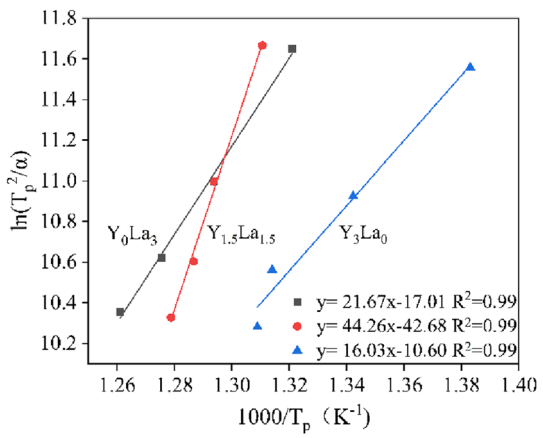

Fig. 4 Crystallographic peaks of $\ln(T_p^2/\alpha)$~$1000/T_p$ in glass samples.

crystallization of Y_3La_0 is three-dimensional. Using the Kissinger method to calculate activation energies in three-component glasses, it was found that the Y_2O_3-only doped LAS microcrystalline glass exhibited the lowest activation energy for crystallization. Additionally, the growth index (n) for this glass was greater than 3, indicating a pronounced promotion of crystallization. By contrast, the La_2O_3-only doped LAS and La_2O_3 and Y_2O_3 co-doped LAS microcrystalline glasses demonstrated a weaker ability to promote crystallization (Table 2).

3.3.3 Kinetic analysis by the iso-conversion method. In isothermal and non-isothermal crystallization kinetics, it is commonly assumed that n and E_c remain constant during glass crystallization.[40] However, some researchers have found that, in practice, the values of n and E_c vary with the nucleation and growth rates during crystal crystallization in the glass, implying that the values of n and E_c may not remain constant for different crystal crystallization integrals in isothermal or non-isothermal methods.[41] Most solid-phase reactions involve numerous reaction steps, and the activation energy usually varies as the reaction progresses. Accordingly, iso-conversion methods have been proposed for calculating the values of E_c and n:[42]

$$\frac{dx}{dt} = A \exp\left(\frac{-E}{RT}\right) f(x) \quad (5)$$

Assuming that $f(x)$ is a reaction modeled by a constant heating rate $\alpha = dT/dt$ at non-isothermal temperatures, the above equation can be written as

$$\frac{dx}{dt} = \frac{dx}{dT} * \frac{1}{\alpha} = \frac{1}{\alpha} A \exp\left(\frac{-E}{RT}\right) f(x) \quad (6)$$

where the conversion rate can be obtained from the DSC curves shown in Fig. 1 as well as from the crystallinity fraction plots [39]. By utilizing this data, we can calculate the crystal crystallization integral number x at various temperatures for different heating rates, as illustrated in Fig. 5. At any moment, the precipitated crystal integration number x can be obtained by calculating the ratio S_x/S, where S_x is the area of any region between T_1 (start of crystallization) and T_2 (end of crystallization), and S denotes the total area of the crystallization peaks.

3.3.4 Kissinger–Akahira–Sunose (KAS) model. Even if the function $f(x)$ is unknown, it is still possible to ascertain the effective activation energy of any reaction process for a specific value of the crystallinity fraction x. The value of E remained constant for the same crystallinity condition at different reaction temperatures. Fig. 5 displays the heating rate temperature functions corresponding to various degrees of crystallinity. Following the definition of the above equation for the iso-conversion method, the KAS model can be expressed as

$$\ln\left(\frac{T_x^2}{x}\right) = \frac{E_c}{RT_x} + C_2 \quad (7)$$

Table 2 Crystallization growth indices of the samples

Heating rates sample	Y_0La_3	$Y_{1.5}La_{1.5}$	Y_3La_0
5	1.49	1.37	5.53
10	1.57	1.35	4.67
15	1.63	1.51	4.27
20	1.80	1.27	3.79

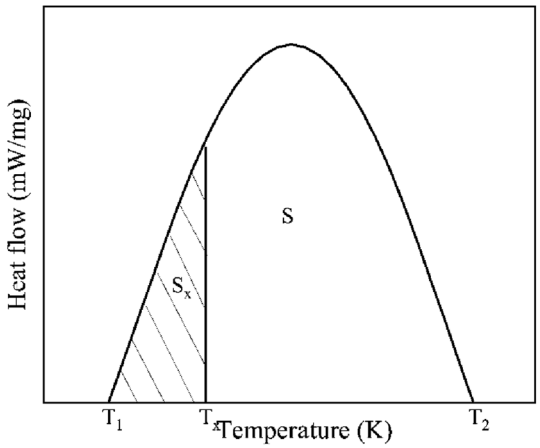

Fig. 5 Schematic diagram of DSC crystallinity × calculation method.

As shown in Fig. 6, the graph represents the relationship between crystallinity and temperature, demonstrating the temperature dependence of crystallinity x. The temperature T_x corresponds to a crystallinity fraction of x. Fig. 6 shows the temperature function of the heating rate corresponding to different conversions for three samples according to the DSC peaks to make the image of $1000/T_x - \ln(T_x^2/x)$ at different x. After fitting, $E_{c(x)}$ can be obtained (Fig. 7).

For $n_{c(x)}$, this can be calculated by the following equations:[43,44]

$$n_{c(x)} = -\frac{R}{E_c(x)} * \frac{\Phi \ln[-\ln(1-x)]}{\Phi(1/T)} \quad (8)$$

The graph is first plotted for $1000/T_x - \ln[-\ln(1-x)]$, and then eqn (8) is used to obtain $n_{c(x)}$ (Fig. 8).

As can be seen from Fig. 9, with an increase in the crystallinity fraction x, the Y_0La_3 decreased from 172.36 to 166.89 kJ mol^{-1}, the $Y_{1.5}La_{1.5}$ decreased from 318.58 to 280.66 kJ mol^{-1}, and the Y_3La_0 decreased from 183.69 to 135.68 kJ mol^{-1}, indicating that the activation energy of crystallization decreases over time. This trend suggests that the activation energy of crystallization decreased over time. The activation energy of crystallization acts as a barrier for the glass, and the three samples exhibited diminishing resistance to crystallization from the initial stages to the later stages of crystallization. $E_{c(x)}$ generally consists of two parts: the activation energy of nucleation, E_n, and the activation energy of growth, E_g.[45]

$$E_{c(x)} = aE_n + bE_g \quad (9)$$

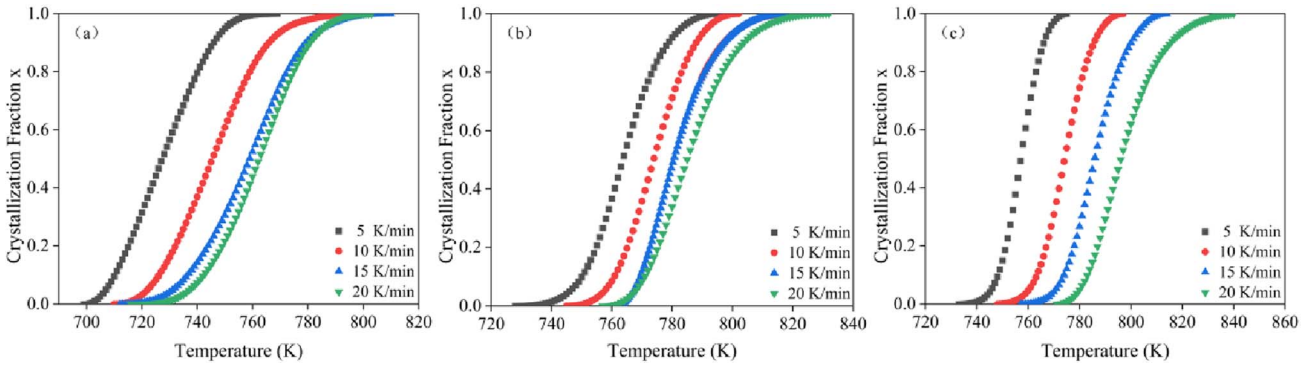

Fig. 6 (a–c) Crystallinity fraction x as a function of temperature for Y_0La_3, $Y_{1.5}La_{1.5}$, and Y_3La_0 glass samples at different heating rates.

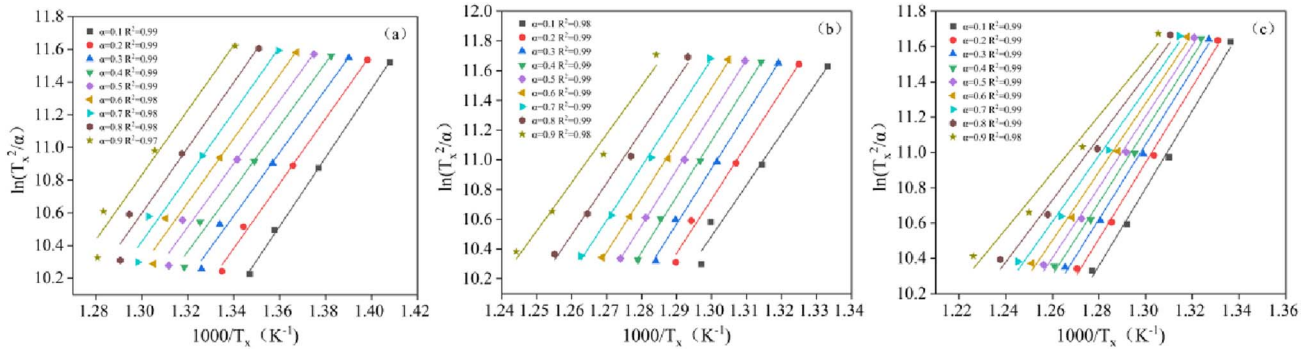

Fig. 7 (a–c) $\ln(T_\alpha^2/\alpha) \sim 1000/T_x$ plots of crystallinity fractions x of Y_0La_3, $Y_{1.5}La_{1.5}$ and Y_3La_0 glass samples.

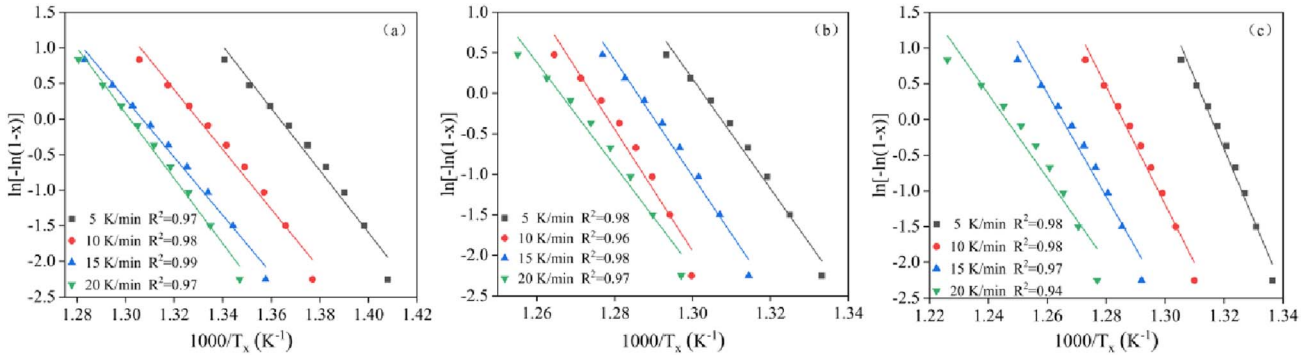

Fig. 8 (a–c) Plots of $\ln[-\ln(1-x)] \sim 1000/T_x$ for Y_0La_3, $Y_{1.5}La_{1.5}$ and Y_3La_0 glass samples at different heating rates.

As shown in Fig. 9, $n_{c(\alpha)}$ increased with the crystallization fraction for all three sample glasses. For the sample glasses doped solely with Y_2O_3, as well as those co-doped with Y_2O_3 and La_2O_3, $n_{c(x)}$ was within the range of 1.7 to 2.4 at different heating rates. This observation suggests that the samples initially began as one-dimensional crystallites and then rapidly evolved into two-dimensional crystallites.[37] However, for Y_2O_3 doped with 3 mol, the initial $n_{c(x)} > 2.3$ reached two-dimensional crystallization from the beginning, followed by a gradual evolution to three-dimensional crystallization or even higher. Furthermore, the activation energies for crystallization in all three component glasses were within the 121–331 kJ mol^{-1} range. Consequently, the glass system has sufficient time and capacity to undergo nucleation and crystallization.

3.3.5 Friedman (FR) model. The method of calculation based on the conversion rate at T_x (α) and the data at T_x (α) is called Friedman's method. The FR model represents a differential iso-conversion model that does not rely on specific assumptions when calculating the activation energy for a constant crystallinity fraction during the non-isothermal transformation process, which is integrated over eqn (6), and for different crystallinity fractions x, the Friedman equation[46] is obtained as

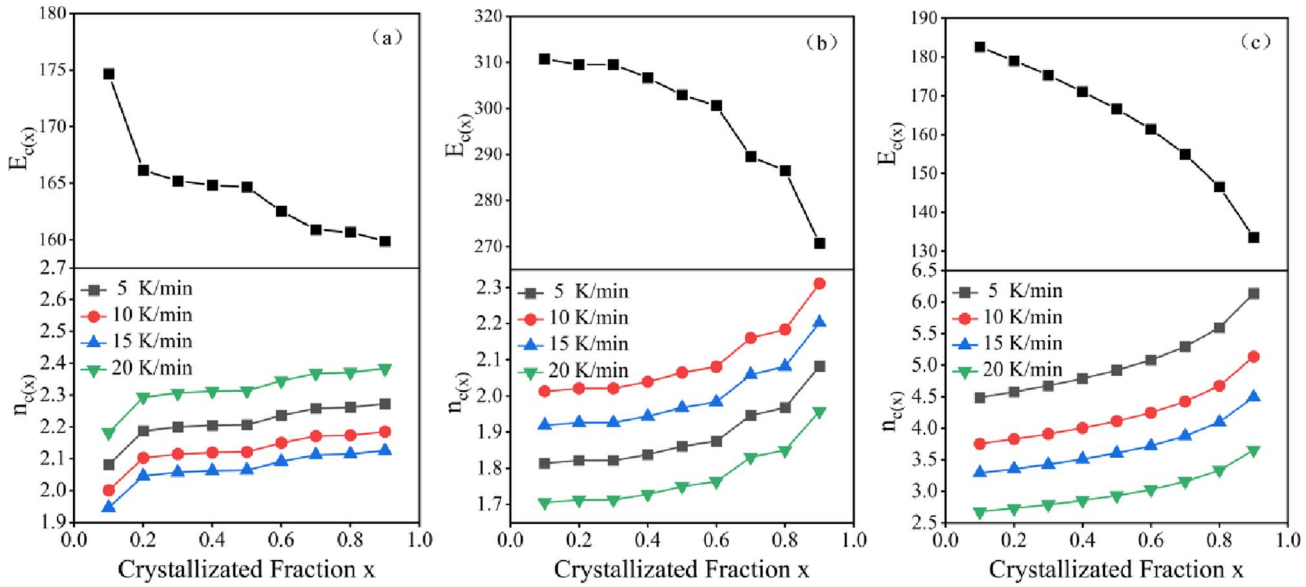

Fig. 9 (a–c) Plots of $E_{c(\alpha)}$ and $n_{c(\alpha)}$ as a function of crystallization fraction α corresponding to Y_0La_3, $Y_{1.5}La_{1.5}$ and Y_3La_0 glass samples.

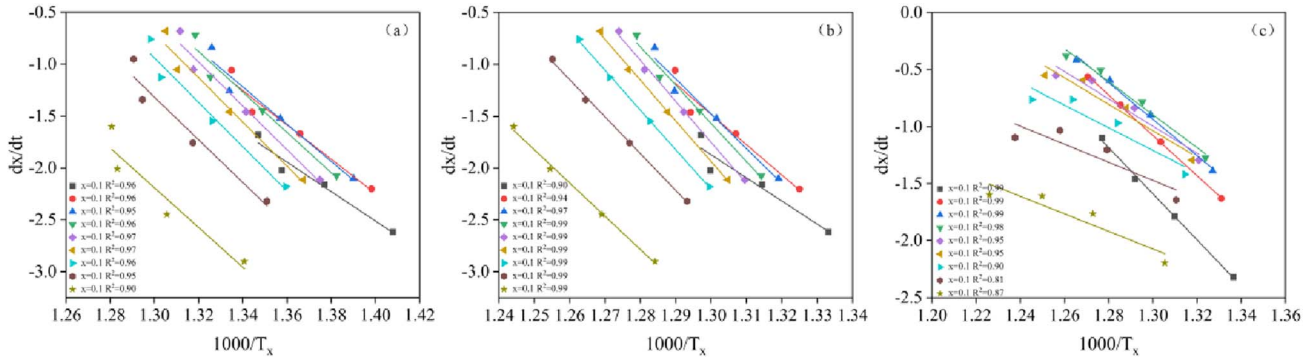

Fig. 10 (a–c) dx/dt *vs.* 1000/T_x plots for Y_0La_3, $Y_{1.5}La_{1.5}$ and Y_3La_0 glass samples.

$$\ln\left(\alpha^{*}\frac{\mathrm{d}x}{\mathrm{d}T}\right)_{x,i} = \ln\left[A_x{*}f(x)_i\right] - \frac{E_c}{RT_{x,i}} \qquad (10)$$

The fitted curves of dx/dT *versus* crystallinity fractions ranging from 0.1 to 0.9 for the three samples are presented in Fig. 10. The activation energy (E_x) was determined by calculating the slope of the least-squares fit. As shown in Fig. 11, the activation energy of crystallization varied with the change in conversion. Specifically, the value of $E_{(x)}$ remained relatively constant with the conversion, but the activation energy exhibited a decreasing trend. It is worth noting that the activation energy reached its highest point when the crystallinity was at 0.1. The activation energies of the three samples, obtained using both the KAS and FR methods, were compared and analyzed. Notably, the activation energies exhibited a consistent trend, decreasing with the increase in the fraction of crystallinity. Among the activation energies of the three components calculated by these two methods, the La_2O_3 doped LAS glass exhibited the highest activation energy of crystallization, indicating that it is more difficult to crystallize and possesses good stability. Conversely, the Y_2O_3 doped glass showed the lowest activation energy of crystallization, suggesting that the Y_2O_3 doped LAS glass had the smallest potential barriers to overcome during crystallization and was more conducive to the crystallization

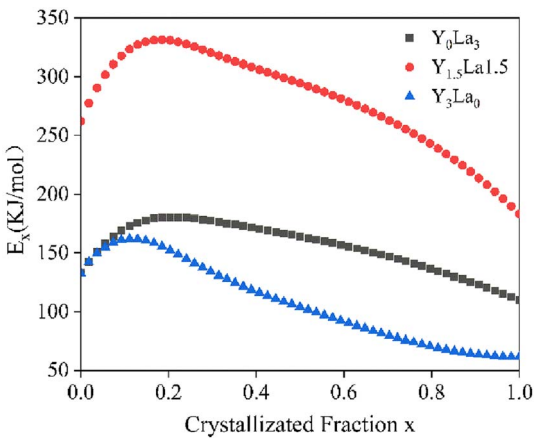

Fig. 11 Calculated activation energies of glass samples with different compositions by Friedman's method.

process compared with the other two glass components. Furthermore, it is evident that all three glass components can undergo two-dimensional crystallization based on the calculated growth indices of crystallization. Remarkably, the Y_3La_0 component of the glass, with a significantly lower activation energy of crystallization, can even achieve three-dimensional crystallization.

4 Conclusions

The crystallization kinetics of rare-earth Y_2O_3 and La_2O_3 doped LAS glass ceramics were explored under non-isothermal conditions. The precipitated crystalline phases during the crystallization process were analyzed using XRD and SEM techniques. Subsequently, the crystallization kinetic parameters of the three component glasses were successfully calculated using the model-fitting method (Kissinger) and the model-free methods (Kissinger–Akahira–Sunose and Friedman).

The results revealed that the crystalline phase of β-quartz solid solution precipitated from all rare earth element-doped LAS glasses under conditions without nucleating agents. Moreover, the crystallization trend remained consistent for LAS glasses, regardless of the method used for calculation. Accurate kinetic calculations showed that the corresponding activation energies of crystallization were 133.24 kJ mol^{-1}, 354.81 kJ mol^{-1}, and 180.23 kJ mol^{-1} when the Kissinger method was used. The KAS method indicated that the local activation energies at the beginning of crystallization were 172.36 kJ mol^{-1}, 318.58 kJ mol^{-1}, and 183.69 kJ mol^{-1}. The activation energies calculated by both the KAS and Friedman methods decreased with the increase in the degree of crystallinity, whereas the Friedman method indicated a maximum activation energy of crystallization at a degree of crystallinity of 0.1. In addition, the Avrami index $n_{c(x)}$ had a significant tendency to increase with increasing degree of crystallinity. As calculated using different methods, the crystallization trend of the three components of LAS glasses remained consistent. The LAS glass doped with only La exhibited the highest activation energy of crystallization among the three methods, suggesting that this glass component encounters the most significant potential barrier during crystallization. In contrast, the LAS glass doped with only Y_2O_3 displayed the lowest activation energy of crystallization, indicating that this component had a strong tendency for crystallization. In this experiment, the glass doped with rare earth oxides, namely Y_2O_3 and La_2O_3, crystallized *via* two-dimensional or three-dimensional growth based on an undoped nucleating agent, the rare earth Y_2O_3 and La_2O_3 could promote the crystallization of LAS glass, and the microcrystalline glass doped with only Y_2O_3 crystallized the best. In future research, analyzing the effect of the remaining rare earth elements on glass crystallization under the condition of undoped nucleating agents can provide insights for the further development of rare earth elements and new materials.

Author contributions

Conceptualization: Tao Zheng, Hong Jiang; formal analysis: Tao Zheng, Minghan Li; funding acquisition: Hong Jiang, Yanping Ma; project administration: Hong Jiang; supervision: Hong Jiang, Yanping Ma; visualization: Tao Zheng; writing-original draft: Tao Zheng; writing-review and editing: Tao Zheng, Minghan Li, Yanping Ma and Hong Jiang.

Conflicts of interest

There are no conflicts to declare.

Acknowledgements

This work is supported by the Key Scientific & Technological Project of the Hainan Province (ZDKJ2021049), Joint Fund Project of the National Natural Science Foundation of China (U22A20124). The funding agency had no role in the study design; in the collection, analysis and interpretation of data; in the writing of the report; and in the decision to submit the article for publication.

References

1 C. Venkateswaran, H. Sreemoolanadhan and R. Vaish, *Int. Mater. Rev.*, 2022, **67**, 620.
2 E. D. Zanotto, *Am. Ceram. Soc. Bull.*, 2010, **89**, 19.
3 H. Savabieh, P. Alizadeh, Y. A. R. Dasilva, R. Erni and F. J. Clemens, *J. Eur. Ceram. Soc.*, 2017, **37**, 631.
4 S. Wang, F. Kuang, Q. Ye, Y. Wang, M. Tang and C. Ge, *J. Mater. Sci.*, 2016, **32**, 583.
5 L. Lilensten, Q. Fu, B. R. Wheaton, A. J. Credle, R. L. Stewart and J. T. Kohli, *Ceram. Int.*, 2014, **40**, 11657.
6 S. Xu, F. Jia, G. Zhang, T. Zhao, H. Zhang and C. Su, *J. Non-Cryst. Solids*, 2022, **581**, 121436.
7 L. S. Gallo, F. Célarié, N. Audebrand, A. C. M. Rodrigues, E. D. Zanotto and T. Rouxel, *J. Am. Ceram. Soc.*, 2017, **100**, 2166.
8 L. Arnault, M. Gerland and A. Rivière, *J. Mater. Sci.*, 2000, **35**, 2331.
9 S. Ueno, S. Tsutaki, N. Kan-no, C. Sunghun and T. Sekino, *Mater. Today: Proc.*, 2023, DOI: **10.1016/j.matpr.2023.05.413**.
10 S. M. Salman, S. N. Salama and E. A. Mahdy, *Bol. Soc. Esp. Ceram. Vidrio*, 2019, **58**, 94.
11 O. B. Petrova, D. A. Velichkina, M. P. Zykova, A. V. Khomyakov, M. A. Uslamina, K. N. Nischev, A. A. Pynenkov, R. I. Avetisov and I. Ch. Avetissov, *J. Non-Cryst. Solids*, 2020, **531**, 119858.
12 A. Chakrabarti, K. Biswas and A. R. Molla, *J. Alloys Compd.*, 2018, **740**, 237.
13 S. Ahmad, M. Herrmann, M. M. Mahmoud, H. Leiste, W. Lippmann and H. J. Seifert, *J. Alloys Compd.*, 2016, **688**, 762.
14 L. Baowei, Z. Ming, Z. Xuefeng, C. Hua and D. U. Yongsheng, *Mater. Rev.*, 2012, **26**, 44.
15 G. H. Chen, J. L. Li, Y. Yang, C. L. Yuan and C. R. Zhou, *Mater. Res. Bull.*, 2014, **50**, 141.
16 D. J. H. F. Wei, *J. Inorg. Mater.*, 2007, **22**, 35.
17 L. Chen, C. Yu, L. Hu and W. Chen, *J. Non-Cryst. Solids*, 2013, **360**, 4.

18 A. Arvind, A. Sarkar, V. K. Shrikhande, A. K. Tyagi and G. P. Kothiyal, *J. Phys. Chem. Solids*, 2008, **69**, 2622.
19 T. R. Rao, C. V. Reddy, C. R. Krishna, U. S. U. Thampy, R. R. Raju, P. S. Rao and R. V. S. S. Ravikumar, *J. Non-Cryst. Solids*, 2011, **357**, 3373.
20 H. Wen and P. A. Tanner, *J. Alloys Compd.*, 2015, **625**, 328.
21 S. S. A. Qazvini, Z. Hamnabard, Z. Khalkhali, S. Baghshahi and A. Maghsoudipour, *Ceram. Int.*, 2012, **38**, 1663.
22 J. Wang, C. Liu, G. Zhang, J. Xie, J. Han and X. Zhao, *J. Non-Cryst. Solids*, 2015, **419**, 1.
23 G. Kaur, M. Kumar, A. Arora, O. P. Pandey and K. singh, *J. Non-Cryst. Solids*, 2011, **357**, 858.
24 D. Wei and L. U. Jin-Shan, *Trans. Mater. Heat Treat.*, 2011, **32**, 19.
25 X. Li, Y. Wang, P. Yang, T. Han, X. Shi, K. He and C. Zu, *J. Non-Cryst. Solids*, 2022, **596**, 121847.
26 A. Prnová, A. Plško, R. Klement, J. Valúchová, K. Haladejová, P. Švančárek, M. Majerová and D. Galusek, *J. Non-Cryst. Solids*, 2018, **501**, 55.
27 S. Machida, K. Katsumata, K. Maeda and A. Yasumori, *ACS Omega*, 2023, **8**, 8766.
28 X. Huang, D. Zhao, L. Ma, C. Deng, L. Li, K. Chen and X. Yang, *J. Non-Cryst. Solids*, 2020, **536**, 120007.
29 W. Zheng, J. Cheng, L. Tang, J. Quan and X. Cao, *Thermochim. Acta*, 2007, **456**, 69.
30 M. S. Shakeri, *Int. J. Miner., Metall. Mater.*, 2013, **20**, 450.
31 M. Cable and J. Hakim, *Chem. Eng. Sci.*, 1972, **27**, 409.
32 F. Liu, F. Sommer, C. Bos and E. J. Mittemeijer, *Int. Mater. Rev.*, 2007, **52**, 193.
33 W. A. Johnson, *Trans. Am. Inst. Min. Metall. Eng.*, 1939, **135**, 416.
34 D. W. Henderson, *J. Non-Cryst. Solids*, 1979, **30**, 301.
35 M. Avrami, *J. Chem. Phys.*, 1940, **8**, 212.
36 K. Matusita and S. Sakka, *J. Non-Cryst. Solids*, 1980, **38**, 741.
37 T. Ozawa, *Bull. Chem. Soc. Jpn.*, 1965, **38**, 1881.
38 H. E. Kissinger, *J. Res. Natl. Bur. Stand.*, 1956, **57**, 217.
39 J. A. Augis and J. E. Bennett, *J. Therm. Anal.*, 1978, **2**, 283.
40 A. A. Abu-Sehly, S. N. Alamri and A. A. Joraid, *J. Alloys Compd.*, 2009, **476**, 348.
41 A. A. Joraid, S. N. Alamri and A. A. Abu-Sehly, *J. Non-Cryst. Solids*, 2008, **354**, 3380.
42 T. Akahira and T. Sunose, *Res. Rep. Chiba Inst. Technol.*, 1971, **16**, 22.
43 M. Abu El-Oyoun, *J. Alloys Compd.*, 2009, **486**, 1.
44 A. Srivastava, N. Chandel and N. Mehta, *Heliyon*, 2017, **3**, e249.
45 H. Yinnon and D. R. Uhlmann, *J. Non-Cryst. Solids*, 1983, **54**, 253.
46 M. Salehi, F. Clemens, T. Graule and B. Grobéty, *Appl. Energy*, 2012, **95**, 147.